

Linewidths and energy shifts of electron-impurity resonant states in quantum wells with infinite barriers

Pavel A. Belov ^{*}*Spin Optics Laboratory, St. Petersburg State University, Ulyanovskaya 1, 198504 St. Petersburg, Russia*

(Received 26 October 2021; revised 15 April 2022; accepted 18 April 2022; published 26 April 2022)

The linewidths and the energy shifts of the resonant states of the impurity electron in GaAs-based quantum wells (QWs) with infinite barriers are calculated. The two-dimensional Schrödinger equation for the charge impurity in the QW is solved by the developed finite-difference method combined with the complex-scaling technique. A dependence of the linewidths and energy shifts on the QW width for the impurity localized in the center of the QW is studied. The calculated results extend and improve theoretical estimations of these quantities in the GaAs-based QW by Monozon and Schmelcher [*Phys. Rev. B* **71**, 085302 (2005)]. In particular, in agreement with their studies we obtain that resonant states originating from the second quantum-confinement subband have negligibly small linewidths. In contrast to previous estimations, we show that for the QW widths of the order of the electron impurity's Bohr radius the linewidths of resonant states associated with the third quantum-confinement subband linearly depend on the thickness of the QW. We show how the previous theoretical predictions can be improved for such QW widths. We also calculate linewidths for the case when the electron impurity is localized away from the center of the QW.

DOI: [10.1103/PhysRevB.105.155417](https://doi.org/10.1103/PhysRevB.105.155417)

I. INTRODUCTION

Many studies have been devoted to the charge impurities and the bound electron-hole pairs, excitons, in semiconductors with a degenerate valence band [1–4]. The early experimental works have mainly addressed the fundamental properties of these quasiparticles, namely the lifetime and the radiative characteristics, as well as the ways to tune them by confining in heterostructures with quantum wells (QWs) [5–8]. The renewed interest in these structures is based on certain applications, in particular, on the quantum-cascade lasers [9–11] as the primary sources of the terahertz radiation [12–17].

From the theoretical point of view, charge carriers and excitons in heterostructures with QWs are interesting model systems, allowing for an accurate theoretical treatment and comparison with experiment. Since the first works of Bastard on the charge impurities [18,19] and following numerous works on excitons in QWs [20–28], the variational calculations of bound state energies have become a standard approach. Most of the variational studies were devoted to the ground state energy since the simplest choice of the trial function in the variational method (see for example Refs. [21,27,29,30]) allows one to reliably simulate only the ground state. To calculate the energy levels of the excited states, for example originating from upper quantum-confinement subbands in QW, one needs the specially chosen set of trial functions that complicates numerical solution.

In order to simplify the problem, some works investigated the bound states in very narrow QWs, when the Coulomb potential can be effectively treated as a two-dimensional (2D)

one [31–33]. Another common approximation was to ignore the Coulomb coupling of the bound states at upper subbands with the continuum of lower subbands. In fact, this coupling leads to the resonant (quasibound) states in the continuum which are characterized not only by the energies, but also by the nonzero linewidths.

The resonant states of the charge impurities were investigated both analytically and numerically in several works [34–39]. The most instructive one is Ref. [38], in which Monozon and Schmelcher considered resonances in the model of three quantum-confinement subbands in narrow QW with infinite barriers. For such a case, the perturbative methods allowed them to derive the analytical expressions for energy shifts and linewidths of the resonant states of an impurity electron as well as of an electron-hole pair in a QW of width L . In particular, they obtained that the linewidth scales with L as L^4 , which is in agreement with the Fano theory of resonances [40,41]. This result, however, is applicable only for a model of very narrow QWs, when the QW thickness is much smaller than the Bohr radius a_B of the particle. Thus, the predictions of Ref. [38] may be inappropriate for more realistic conditions. On the one hand, the model of very narrow QWs may be rough even for well-studied structures. In particular, for GaAs-based heterostructures the envelope function approximation is not accurate enough for the QW thicknesses smaller than 3 nm [42,43], whereas for bulk GaAs, the Bohr radius $a_B = \epsilon \hbar^2 / (m_e e^2)$ of the electron impurity is of about 10 nm. On the other hand, for larger L , a behavior of the linewidth is more complicated [44]. The steep fourth-order dependence should quickly mitigate with increase of L , then the linewidth reaches its maximal value and further decreases. It should completely vanish for the model of a bulk semiconductor, as $L \rightarrow \infty$.

^{*}pavelbelov@gmail.com

In the present paper we numerically study the linewidths of the resonant (quasibound) states of the electron impurity in a single QW with infinite barriers. The upper quantum-confinement subbands are coupled to the unrestricted in-plane electron-impurity motion of lower subbands and lead to a resonant nature of the upper states. The resonant states are well known in quantum physics [40,45,46]: the linewidth $\hbar\Gamma$ of the energy level E determines the lifetime of a resonant state. In semiconductor physics, the quasibound states of the electron-hole pairs in QWs are in the scope of intensive studies [26,33,47–49]. There are also works devoted to the bound states in the continuum [50,51] characterized by very small nonradiative broadenings [52]. Nevertheless, it is the non-radiative processes that usually dominate the broadening of the electron-hole resonances, even for high-quality samples. Therefore, the theoretical estimations of the radiative and non-radiative linewidth broadenings are of significant importance for spectroscopy of heterostructures. Since the electron-hole pairs in QWs are effectively three-body systems [53,54], they are more complicated objects than the charge impurities. As a result, before studying the features of electron-hole resonances, one has to investigate resonant states of the charge impurities.

In order to calculate the linewidths, we use the complex-scaling technique [55]. It transforms the scattering problem into the boundary value problem with zero boundary conditions. It was rigorously established for the description of resonance characteristics in the early 1970s [56–59]. Since then, many quantum scattering problems in nuclear and atomic physics have been studied by this technique [60–66]. In semiconductor physics, a feasibility of complex-scaling calculations of the electron-hole nonradiative linewidths was first demonstrated in Ref. [67]. Recently, the complex scaling has also been applied to identify energies and linewidths of the resonant series of the electron-hole pairs in the transition metal dichalcogenides [68] and bulk cuprous oxide [69–71].

We study the resonance characteristics using the developed numerical algorithm combined with the complex-scaling rotation. Our numerical algorithm is based on the finite-difference discretization of the two-dimensional Schrödinger equation. A similar approach has already allowed us to obtain precise exciton energies for a wide range of QW widths and different potential profiles [27,33,47]. In the current work we readily determine the spectrum of the bound and resonant states of the electron impurity localized in the center of the GaAs-based QW. The bulk GaAs material parameters are used in calculations [72]. Using the complex-scaling technique, we distinguish the proper states from the artificially discretized continuum, and classify the resonant states over the quantum-confinement subbands. A dependence of the linewidths of resonant states on the QW width and the index of the subband is studied. In particular, we obtain that the resonant states associated with the second quantum-confinement subband have negligibly small linewidths. Thus, they have very long lifetime and can be considered as an example of the bound states in the continuum. We extend the results presented by Monozon and Schmelcher for very narrow QWs to wider ones by providing new calculated data on the linewidths of resonant states of the third quantum-confinement subband for QWs widths L up to 150 nm. We also show that in order to obtain more precise

linewidths for QW widths of order of the Bohr radius one can use the complete formulas derived in Ref. [38] without approximations, which the authors then employed to achieve the final analytical expressions of Ref. [38]. Additionally, we calculate linewidths for the case when the electron impurity is localized away from the center of the QW.

II. THEORY

A. The energy levels of the electron impurity in the QW

We consider an electron impurity (a donor center) localized at the distance b from the center of the QW. The z axis is chosen along the growth axis and $\vec{\rho}$ is the radius vector in the QW plane. The point $z = 0$ is in the center of the QW. Within the effective mass approximation, the wave function of the electron impurity at the position $\mathbf{r}(\vec{\rho}, z)$ satisfies the time-independent Schrödinger equation [38]

$$\left(-\frac{\hbar^2}{2m_e} \Delta - \frac{e^2}{\epsilon \sqrt{|\vec{\rho}|^2 + (z-b)^2}} + V_e(z) \right) \Psi(\mathbf{r}) = E \Psi(\mathbf{r}). \quad (1)$$

Here Δ is the three-dimensional Laplace operator, m_e is the electron mass, e^2 is the square of the electron charge, and ϵ is the dielectric permittivity constant. The QW potential $V_e(z)$ is defined as

$$V_e(z) = \begin{cases} 0 & \text{if } |z| < L/2, \\ \infty & \text{if } |z| \geq L/2. \end{cases} \quad (2)$$

To simplify Eq. (1), we introduce the polar coordinates $\vec{\rho} = (\rho, \phi)$ within the QW plane. Separating the angle variable and taking into account only cylindrically symmetrical solutions, Eq. (1) is reduced to the two-dimensional equation

$$\left(-\frac{\hbar^2}{2m_e} \frac{\partial^2}{\partial z^2} + V_e(z) - \frac{e^2}{\epsilon \sqrt{\rho^2 + (z-b)^2}} - \frac{\hbar^2}{2m_e} \left[\frac{\partial^2}{\partial \rho^2} - \frac{1}{\rho} \frac{\partial}{\partial \rho} + \frac{1}{\rho^2} \right] \right) \chi(\rho, z) = E \chi(\rho, z), \quad (3)$$

where the function $\chi(\rho, z)$ is related to the radial part of the wave function $\Psi(\rho, z)$ as $\chi(\rho, z) = \rho \Psi(\rho, z)$.

The energy levels of the electron impurity in the QW are governed by Eq. (3). The scheme of energy levels can be easily obtained for the model of a very narrow QW. In such a case, the initial Coulomb-like potential becomes effectively two dimensional, $-e^2/(\epsilon\rho)$, and the variables in the equation can be separated. The resulted energy spectrum is shown in Fig. 1. In the figure, the quantum-confinement subbands, originating from a quantization in the QW, are shown by long horizontal lines. They are defined as [73]

$$E_{ej} = \frac{\hbar^2}{2m_e} \left(\frac{\pi j}{L} \right)^2. \quad (4)$$

Corresponding quantum-confinement wave functions are [4]

$$\psi_j(z) = \sqrt{\frac{2}{L}} \begin{cases} \cos(j\pi z/L) & \text{if } j = 1, 3, 5, \dots, \\ \sin(j\pi z/L) & \text{if } j = 2, 4, 6, \dots \end{cases} \quad (5)$$

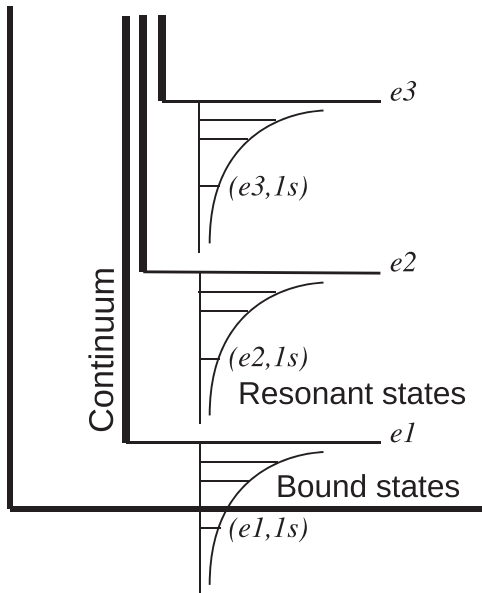


FIG. 1. Scheme of the energy levels of the impurity electron in a very narrow QW with infinite barriers. The quantum-confinement subbands e_j , $j = 1, 2, 3$, as well as the corresponding branches of the continuum are shown. The bound and resonant states are explicitly denoted.

Below each quantum-confinement subband, there is a set of the 2D Coulomb potential energy levels [32,33]

$$E_N^C = -\frac{4 \text{ Ry}}{(2N - 1)^2}. \quad (6)$$

Here $\text{Ry} = m_e e^4 / (2\epsilon \hbar^2)$ is the Rydberg energy of the impurity electron in bulk GaAs.

As a result, we can classify the energy levels by the index $j = 1, 2, 3, \dots$ of the quantum-confinement subband as well as by the principal quantum number $N = 1, 2, 3, \dots$ of the Coulomb-like level: (e_j, N_s) . For example, the lowest energy level is $(e1, 1s)$, see Fig. 1. It is worth noting that for the model of a very narrow QW these numbers are the good quantum numbers.

Below the lowest quantum-confinement subband $e1$, there are energy levels corresponding to the square-integrable solutions. They are associated with the discrete part of the spectrum. The continuous part of the spectrum takes place above the subband $e1$. Energies of the continuum correspond to the square-nonintegrable, scattering solutions of Eq. (3), i.e., solutions which propagate far away from the interaction domain.

It is important that the Coulomb-like potential of Eq. (3) couples the quantum-confinement subbands. The above-proposed classification and the introduced good quantum numbers are, in fact, approximate. They specify the dominant admixture to a given state. Nevertheless, the introduced classification is convenient in practice until the quantum-confinement quantization is stronger than the Coulomb-like one [33]. This is valid for relatively small L . As L increases, the quantum-confinement quantization becomes weaker and the upper subbands gradually descend. At some point, the QW

quantization becomes so small that the Coulomb-like sets of different subbands start to overlap.

The Coulomb-like energy levels of upper quantum-confinement subbands are coupled to the continuum of the lower subbands. Thus, these states are the resonant (quasibound) states. They are characterized not only by the energy, but also by the linewidth broadening, determining the lifetime of a resonant state. The time evolution of resonant (quasibound) states can be expressed as $\exp[-i(E - i\hbar\Gamma)t/\hbar]$. Therefore, energies E and lifetimes $\tau = \hbar/(2\hbar\Gamma)$ of these states can be defined by complex values with the negative imaginary part $\text{Im}[E] = -\hbar\Gamma$. Here $\Gamma > 0$ is the half-width at the half-maximum (HWHM) linewidth broadening of a resonance [4,27]. It is related to the full-width at the half-maximum (FWHM) definition [73] of broadening as $\Gamma_{\text{FWHM}} = 2\Gamma$.

B. Analytical results on the energy shifts and linewidth broadenings

Due to the Coulomb coupling of the upper subbands with the lower ones as well as with the continuum of lower subbands one obtains the shifts of energy levels and the linewidth broadenings, respectively. In Ref. [38] these quantities were obtained analytically based on the model of the two and three quantum-confinement subbands in a narrow QW with infinite barriers. In the framework of the two-subband model Monozon and Schmelcher obtained the following energies of the Coulomb-like series associated with the second subband $e2$. In our notation they are

$$E_{e2, N_s} = E_{e2} + E_N^C + \Delta E_{e2, N_s} - i\hbar\Gamma_{e2, N_s}, \quad (7)$$

where

$$\Delta E_{e2, N_s} = \frac{8 \text{ Ry}}{(2N - 1)^3} \left(\frac{L}{a_B} \right) \quad (8)$$

and

$$\hbar\Gamma_{e2, N_s} = 0. \quad (9)$$

Here we fixed $b = 0$ to significantly simplify the analytical formulas. We outline the original expressions of Ref. [38] in the Appendix. The first two terms in Eq. (7) refer to the model of a very narrow QW, when the Coulomb potential becomes effectively two dimensional, $\sim -\rho^{-1}$. The energy shift $\Delta E_{e_j, N_s}$ is caused by the effect of the three-dimensional Coulomb potential $\sim (\rho^2 + z^2)^{-1/2}$, compared to that from the two-dimensional one. The zero linewidth $\hbar\Gamma_{e2, N_s}$ originates from the different parity of the wave function of the subband $e2$ with respect to $e1$ (and also to $e3$). The matrix element of the Coulomb potential calculated for these states is exactly zero. Meanwhile, for $b \neq 0$ such a degeneracy is lifted and $\hbar\Gamma_{e2, N_s}$ becomes nonzero.

The energies of the Coulomb-like set of the third quantum-confinement subband $e3$ are

$$E_{e3, N_s} = E_{e3} + E_N^C + \Delta E_{e3, N_s} - i\hbar\Gamma_{e3, N_s}, \quad (10)$$

where

$$\Delta E_{e3, N_s} = \left(1 - \frac{4}{9\pi^2} \right) \left[1 + \frac{4}{\pi^4} \left(\frac{L}{a_B} \right)^2 \right] \frac{8 \text{ Ry}}{(2N - 1)^3} \left(\frac{L}{a_B} \right) \quad (11)$$

and

$$\hbar\Gamma_{e3,Ns} = \left(1 - \frac{4}{9\pi^2}\right) \left[1 - \frac{4}{\pi^2}\right] \frac{8 \text{ Ry}}{\pi^3(2N-1)^3} \left(\frac{L}{a_B}\right)^4. \quad (12)$$

Thus, the linewidths of the energy levels associated with the third subband are nonzero. The quantum-confinement wave function of this subband is of the same parity as that of the first one. In fact, the linewidth $\hbar\Gamma_{e3,Ns}$ appears to be proportional to L^4 , which is in accordance with the Fano theory [38,40].

It is worth noting that Eqs. (7)–(12) are obtained using the following approximations: (1) a few quantum-confinement subbands are taken into account; and (2) very narrow QWs, $L \ll a_B$, are considered. In the present work we study QWs of various widths. We obtain the energy shifts and linewidths numerically without mentioned approximations. Moreover, we consider the original Eq. (3), which means that many quantum-confinement subbands are taken into account.

C. Complex-scaling technique

For simple textbook models, e.g., one-dimensional QWs, the resonance positions and, in particular, the linewidths can be determined analytically relatively easy [55,73,74]. For more complicated systems, the analytical derivation of resonance characteristics is less straightforward (see, for example, Ref. [38] to realize the faced problems). The main point is that, unlike the bound states, the quasibound (resonant) ones are not represented by the square-integrable solutions of the Schrödinger equation. As a result, their energies are beyond the discrete spectrum of the Hamiltonian and the conventional variational methods become inappropriate for treatment of scattering solutions.

The reliable method for calculation of resonance broadenings, the complex-scaling technique, has been established in Refs. [56–59] in the 1970s. Since then, many quantum scattering problems in nuclear and atomic physics have been studied by this technique [55,60–66,75,76]. It states that the complex energies of resonant states can be identified in the discrete spectrum of the non-Hermitian Hamiltonian $H_\theta = H[r \exp(i\theta)]$, obtained from the initial one $H(r)$ by scaling of the coordinate as

$$r \rightarrow r \exp(i\theta). \quad (13)$$

Here $\theta > 0$ is the scaling angle, i.e., the angle of a rotation of the coordinate into the complex upper half-plane. Such a scaling allows one to associate resonant states with the discrete spectrum by making the outgoing scattering waves $\sim \exp(i\sqrt{E}r)$ as $r \rightarrow \infty$ to be square-integrable $\sim \exp(i\sqrt{E}r \cos \theta - \sqrt{E}r \sin \theta)$ by the appropriate choice of the angle θ . As a result, the continuous spectrum becomes rotated into the complex lower half-plane by the double angle 2θ . The bound states remain unchanged for arbitrary θ and one can distinguish them from the discretized continuum. If the angle of the rotation θ is large enough, then the unknown complex energies also appear in the sector of the double angle 2θ . If they are independent of the angle of the rotation, they correspond to the resonance positions.

Figure 2 shows an example of the complex scaling of variable ρ of Eq. (3) into the upper complex half-plane. The

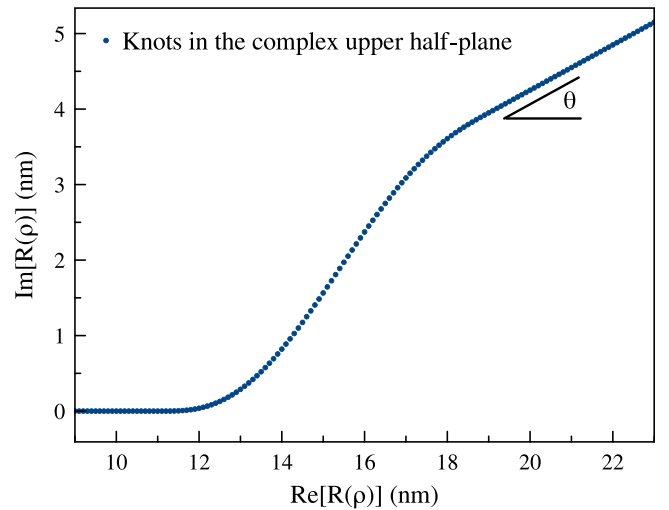


FIG. 2. Knots of the rotated contour for the variable ρ . The smooth exterior complex-scaling rotation is shown. The smooth curve starts at $\rho_0 = 11$ nm and finishes at $\rho_1 = 19$ nm.

figure shows a so-called smooth exterior rotation [63,77] employed in the current work. It implies a change of the variable ρ to the complex function $R(\rho)$ according to the formula

$$R(\rho) = \begin{cases} \rho & \text{if } \rho < \rho_0, \\ \rho_0 + s(\rho; \theta, \rho_0, \rho_1) & \text{if } \rho_0 \leq \rho < \rho_1, \\ \rho_0 + (\rho - \rho_0) \exp i\theta & \text{if } \rho_1 \leq \rho. \end{cases}$$

In this case, the limiting behavior of $R(\rho)$ as $\rho \rightarrow \infty$ is as it would be for the sharp rotation defined by Eq. (13). However, comparing to the sharp rotation, for the exterior one the derivatives of $R(\rho)$ over ρ in the vicinity of the point $\rho = 0$ are zero. Moreover, we additionally introduced the complex-valued function $s(\rho; \theta, \rho_0, \rho_1)$ which matches two limiting behaviors at the interfaces $\rho = \rho_0$ and $\rho = \rho_1$ and guarantees appropriate smoothness.

D. Numerical method

For the calculation of the linewidths $\hbar\Gamma$, we implemented the complex scaling into our finite-difference method of the numerical solution of Eq. (3). Since our method has already been described in detail in Refs. [27,33], we only briefly mention the key points. In the current case, we use the second-order finite-difference discretization on the equidistant grids over each of two variables of the complex-scaled Eq. (3). It leads to an eigenvalue problem with the sparse block-tridiagonal non-Hermitian matrix [78,79]. Several lowest eigenvalues of this matrix are calculated by the Arnoldi algorithm [80]. As a result, we were able to compute the energies and the linewidths of the impurity resonances in QWs of various widths. We used the material parameters for bulk GaAs which are given in Refs. [33,72]: $m_e = 0.067 m_0$ and $\epsilon = 12.53$.

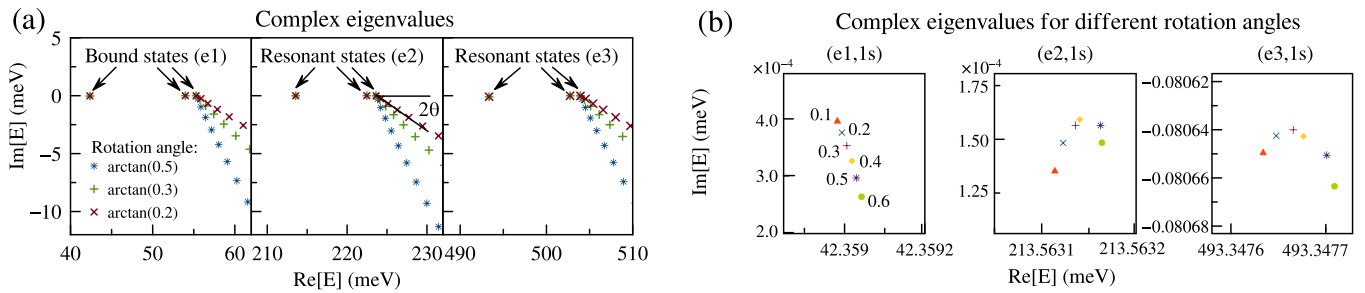


FIG. 3. (a) Calculated eigenvalues of the complex-scaled Eq. (3), defining the states of the electron impurity in the infinite-barrier QW of thickness $L = 10$ nm. Three different angles of the rotation are demonstrated. The left panel shows eigenvalues associated with the lowest quantum-confinement level $e1$, i.e., corresponding to the bound states. The central panel shows the eigenvalues of the energy level $e2$, i.e., the resonant states. The right panel shows the eigenvalues of the quantum-confinement energy level $e3$. The discretized branches of the rotated continuum are also shown. (b) Detailed plots of the calculated eigenvalues of the complex-scaled Eq. (3), defining the electron impurity in the 10-nm QW with infinite barriers. Tangents of the rotation angles θ are also denoted nearby to the corresponding points. The relatively small positive imaginary parts of the complex eigenvalues associated with the subbands $e1$ and $e2$ are due to the uncertainty of the numerical method.

III. RESULTS

A. Dependence of the linewidths on the angle of the rotation

Using our numerical method, we calculated several lowest eigenvalues of the complex-scaled Eq. (3) with $b = 0$ for different QW widths. The smooth exterior rotation of the variable ρ was performed. It started at $\rho_0 = 11$ nm and finished at $\rho_1 = 19$ nm by approaching the straight line inclined by some angle θ to the real axis (see Fig. 2). For example, the numerical results for the QW width $L = 10$ nm are shown in Fig. 3(a) by three panels for better visibility. Each panel corresponds to one set of Coulomb-like energies below the certain quantum-confinement subband e_j , $j = 1, 2, 3$. One can see the branches of the discretized continuum rotated by the double angle 2θ . The complex eigenvalues, independent of θ and corresponding to the bound and resonant states, are explicitly denoted.

The positions of resonances do not depend on the angle of the rotation θ if the numerical scheme is exact. In fact, due to uncertainty of the numerical method, our calculated

series of eigenvalues slightly depend on the rotation angle. To study this dependence we calculated the complex eigenvalues $E - i\hbar\Gamma$ as functions of θ . They are shown in detail in Fig. 3(b). One can see that there is indeed a weak dependence of the results on the angle of the rotation. Moreover, since the bound states should have zero linewidths, we can estimate the accuracy of our calculations as of about 4×10^{-4} meV.

B. Dependence of the energy shift and the linewidth on the thickness of the QW

We calculated the energies of the electron impurity in the infinite-barrier QW of widths $L = 0.6$ –80 nm. To keep the symmetry of the system, we localized the impurity electron in the center of QW ($b = 0$). Comparing calculated energies with the energies $E_{ej} + E_N^C$ for $j = 1, 2, 3$ and $N = 1, 2$, we found the shifts of the energy levels due to the Coulomb coupling. The obtained energy shifts, highlighting the difference of the impurity energy from that in the model of a very narrow QW, are shown for bound and resonant states in Fig. 4(a). One can

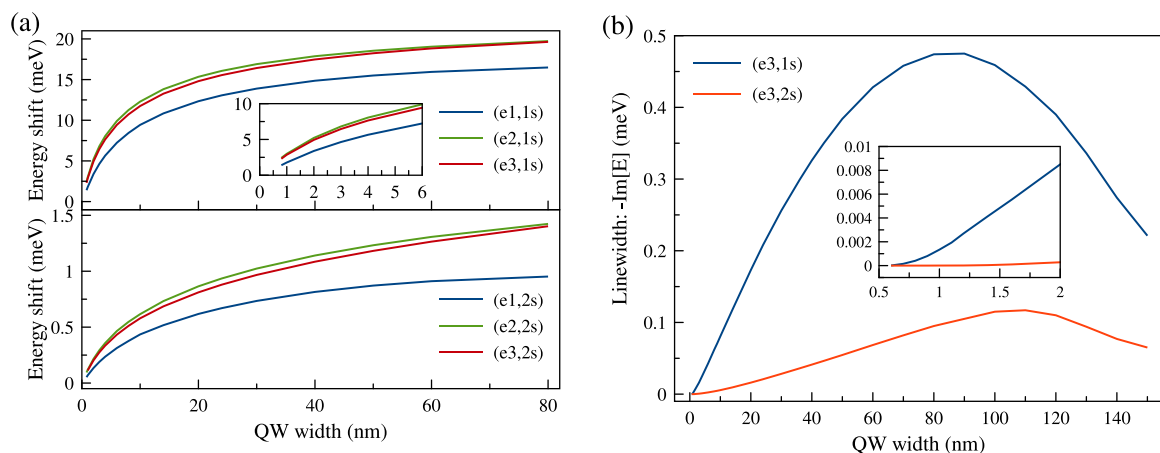


FIG. 4. (a) Calculated energy shifts of the resonant states as well as of the bound states as functions of the QW width. The upper (lower) panel shows the data for $1s$ -like ($2s$ -like) states. The states of the subband $e1$ correspond to the bound states, whereas ones of subbands $e2$ and $e3$ correspond to the resonant ones. (b) Calculated linewidths (HWHM) of the resonant states ($e3, 1s$) and ($e3, 2s$) as functions of the QW width. The insets show the regions of small QW widths in detail.

see that energy shifts grow with an increase of the width of QW. Moreover, for narrow QWs the energy shifts grow faster than for wide QWs. Such a saturation exhibits the fact that the rapid change of energies in the model of 2D Coulomb ($\sim \rho^{-1}$) takes place for narrower QWs, immediately after allowing the electron impurity to move along z axis. For wide QWs, the system is broad enough. Thus, further expansion over z axis weakly affects the energies.

We calculated not only the energies but also the linewidths of the resonant states. Interestingly enough, the widths of the resonant states associated with the second quantum-confinement subband $e2$ appeared to be of the order of the uncertainty of calculations for the whole range of studied QW widths. For example, the complex energy of the state ($e2, 1s$) of order of 10^{-4} meV is shown in the central panel of Fig. 3(b). Therefore, we can numerically confirm the result of Ref. [38] that magnitudes of $\hbar\Gamma_{e2,Ns}$ are negligibly small. Since these states are effectively uncoupled to the continuous spectrum of lower subbands, they can be regarded as the bound states in the continuum [50,52]. By the same reason, they should have sharper, more distinct peaks in the experimental spectra than other resonant states.

The linewidths of the resonant states associated with the third quantum-confinement subband $e3$ are evidently nonzero. These quantities for $1s$ - and $2s$ -like states of this subband are shown in Fig. 4(b) for L up to 150 nm. One can see almost the linear growth of $\hbar\Gamma$ for the $1s$ -like state for QW widths $L = 1.2$ –50 nm. Thus, in agreement with experiments, the states associated with the subband $e3$ should have more pronounced peaks in the measured spectra for narrower QWs [27,28,81]. For wide QWs, $L \sim 100$ nm, the corresponding peaks should be significantly broadened: for such widths the linewidth broadening flattens out and saturates at about 0.5 meV for 80–90 nm. With the further increase of L , $\hbar\Gamma$ gradually reduces and should completely vanish as the energy of the quantum state transfers to the discrete part of the spectrum, below the scattering threshold $e1$ [44].

The linewidth of the $2s$ -like state is, at least, by one order of magnitude smaller than that for the $1s$ -like state, though it shows the similar qualitative dependence on L .

C. Comparison with the analytical results

The results by Monozon and Schmelcher [38] predict that for very narrow QWs, when $L \ll a_B$, the linewidth scales with L as L^4 . In our calculations we can see such a behavior only for very small thicknesses $L = 0.6$ –1.2 nm, see the inset in Fig. 4(b). Since for the electron impurity in bulk GaAs $a_B \approx 10$ nm, this range of L indeed satisfies the above-mentioned criterium. In fact, for these values of L the power-law fit of calculated data gives the dependence $L^{3.5 \pm 0.2}$ which is similar to the theoretical prediction.

Figure 5 shows our numerical results for ($e3, 1s$) resonant state together with the theoretical predictions made by Monozon and Schmelcher as well as calculations performed using the intermediate complete expressions in Ref. [38]. Both theoretical and numerical estimations give relatively small $\hbar\Gamma$ for $L \ll a_B$. However, for $L \sim 0.2a_B$ the complex scaling calculations give values one order of magnitude larger

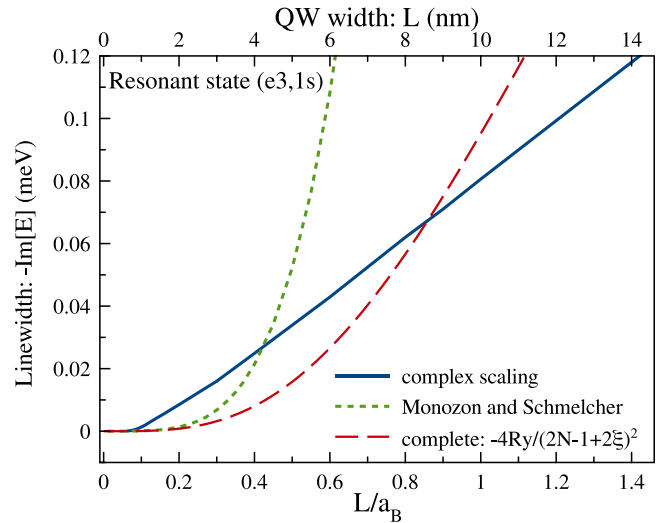


FIG. 5. Calculated linewidths of the resonant state ($e3, 1s$) as functions of L/a_B . Results of our calculations using the complex-scaling technique are shown by the solid line. The linewidths plotted from the final analytical expression of Ref. [38] are denoted by the dotted curve. The linewidths plotted from the intermediate complete expressions of Ref. [38] are shown by the dashed curve.

than the theoretical predictions. Already for such values of L , the complex scaling results show a clear linear dependence, whereas the theoretical predictions of Ref. [38] scale as L^4 for arbitrary widths. With further increase of L , the fourth-order dependence quickly surpasses the linear one. As a result, our numerical data and the values based on the theoretical results by Monozon and Schmelcher significantly differ for $L \sim a_B$.

A discrepancy of the theoretical predictions and our numerical results arises from several approximations employed in Ref. [38]. In particular, the authors approximate the complete expression for the resonance complex energy $E_{e3,Ns} = -4Ry/(2N - 1 + 2\xi)^2$ by the perturbation series

$$E_{e3,Ns} \approx -\frac{4Ry}{(2N-1)^2} + \frac{16Ry \xi}{(2N-1)^3} + \frac{16Ry \xi^2}{(2N-1)^4} \quad (14)$$

with a small parameter ξ , which is, in turn, given by the ratio of perturbation series in powers of L/a_B , see the details in the Appendix. In the leading order, ξ depends linearly on L , therefore for $L \ll a_B$ the shift of energy and the corresponding complex parameter ξ in Eq. (14) are assumed to be small. This allowed the authors of Ref. [38] to take into account only the linear term in Eq. (14) as well as a few lower orders of L/a_B in the perturbation series in both parts of the ratio for ξ . These approximations led finally to the analytical results for the energy shift (11) and the linewidth (12).

Nevertheless, the complete expressions can be used directly without the above-mentioned approximations. It appears that the complete expressions give values [see the dashed curve in Fig. 5] which are closer to the ones calculated by the complex scaling technique. One can see that both results differ by no more than 0.02 meV up until $L \sim a_B$, whereas for such a range the originally predicted L^4

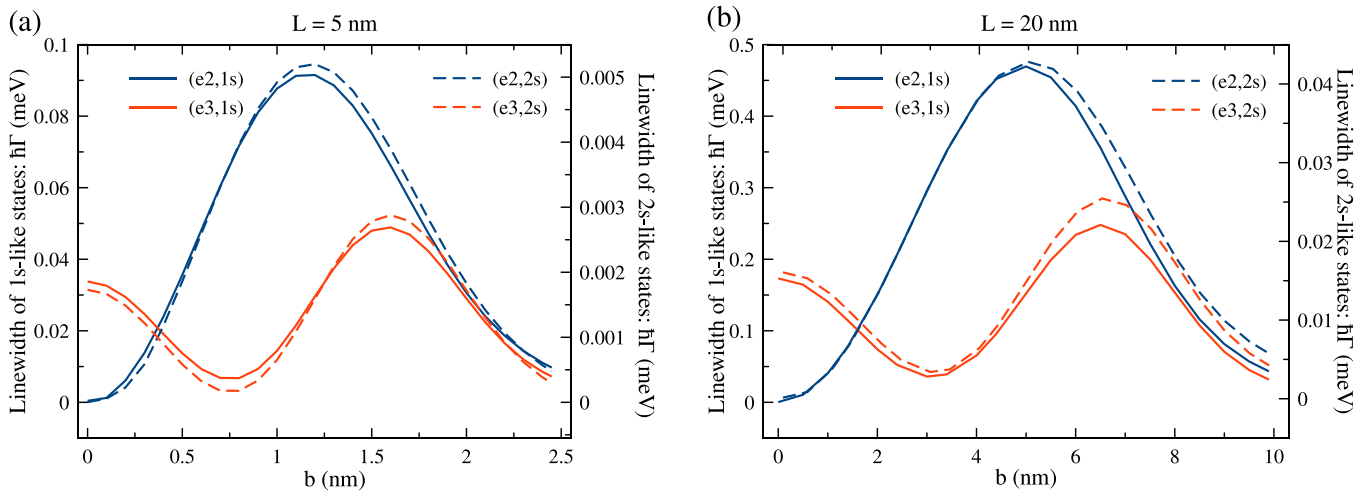


FIG. 6. Calculated linewidths of the resonant states belonging to the second and the third quantum-confinement subbands as functions of the shift b of the impurity from the center of QW. Plot (a) shows data for QW width $L = 5$ nm, whereas plot (b) shows results for $L = 20$ nm.

dependence from Ref. [38] exceeds our numerical data by one order of magnitude.

Interestingly enough, the theoretical predictions in Ref. [38] evidently do not show a linear dependence of $\hbar\Gamma$ on L/a_B , whereas the calculations based on the complete expressions show a linear behavior for $L \sim a_B$. Moreover, the obtained slope of the linear part moderately agrees with the complex scaling result. We can claim that taking into account higher orders of L/a_B in the perturbation series for both parts of the ratio for ξ lead to more pronounced linear dependence on L/a_B . However, the reasons of such a fact require further in depth theoretical studies. Anyway, our numerical calculations do not rely on the perturbation theory and provide accurate results for the whole range of QW widths.

D. Linewidths of the resonant states when the impurity is away from the center of the QW

We additionally studied the case when the electron impurity is away from the center of the QW, i.e., $b \neq 0$. In such a case, a symmetry of the system is broken and, in particular, the linewidths $\hbar\Gamma_{e2,Ns}$ [Eq. (9)] of resonant states associated with the second quantum-confinement subband become nonzero. To show this, we calculated the linewidths as functions of the shift from the center b for different QW widths. The obtained dependencies for $L = 5$ nm and for $L = 20$ nm are shown in Fig. 6. These particular QW widths address the situations when the QW is two times narrower than the electron impurity's Bohr radius and when it is two times wider, respectively. The forms of the dependencies corresponding to the same subbands are approximately the same over the whole range of studied QW widths and differ only by magnitudes. The values of magnitudes for 1s- and 2s-like states are denoted in the plots by the left scale and by the right scale, respectively.

A constant-factor difference in magnitude for 1s- and 2s-like states of the same subbands originates from the general theoretical ratio of the linewidth broadenings Γ_{1s}/Γ_{Ns} , which equals to $(2N - 1)^3$ for the limiting case of the very narrow QW and to N^3 for the bulk semiconductor. In the approximation of Ref. [38], this ratio is independent of b , see exact

formulas in the Appendix. Then, for 1s- and 2s-like states the theoretical ratios in limiting cases should be 3^3 and 2^3 . Since the considered values of L account for the intermediate situations, we numerically obtained for these widths the values of the ratio to be of about 18 and of about 10, respectively. The decrease of the ratio for larger L indicates the crossover from the narrower QW to the wider one.

The detailed analysis of the plots shows that for small $b \sim 0.1$ nm the linewidths $\hbar\Gamma_{e2,Ns}$ for $N = 1, 2$ grow with the increase of b . For larger values of b , the dependencies are nonlinear. They are qualitatively reproduced by the intermediate complete expressions from the paper by Monozon and Schmelcher, whereas further approximations employed by the authors to obtain the analytical formulas lead to less precise results. There are maxima as well as minima of the linewidth broadenings. By varying b one can achieve the situation when the state associated with the subband $e2$ has the maximal linewidth or when that one belonging to the subband $e3$ has the minimal one. The common feature of both plots is that the linewidths become small, when the impurity is localized near the barrier. As it is shown in Ref. [38], the calculated linewidths are related to the matrix elements of the potential. The reduction of $\hbar\Gamma_{e2,Ns}$ originates from the shift of the minimum of the potential close to the barrier, i.e., to the domain where values of the quantum-confinement wave functions in the matrix element are relatively small. Thus, the coupling of the resonant states also becomes small.

IV. CONCLUSIONS AND OUTLOOK

In summary, we calculated the energies and the linewidths $\hbar\Gamma$ of resonant states of the impurity electron in a single QW with infinite barriers. These resonant states originate from the Coulomb coupling of upper quantum-confinement subbands with the continuum of the lower subbands. The two-dimensional Schrödinger equation describing the impurity electron states was solved by the finite-difference discretization method combined with the complex-scaling technique. A dependence of the linewidth broadenings and the energy shifts on the QW width and the index of the quantum-confinement

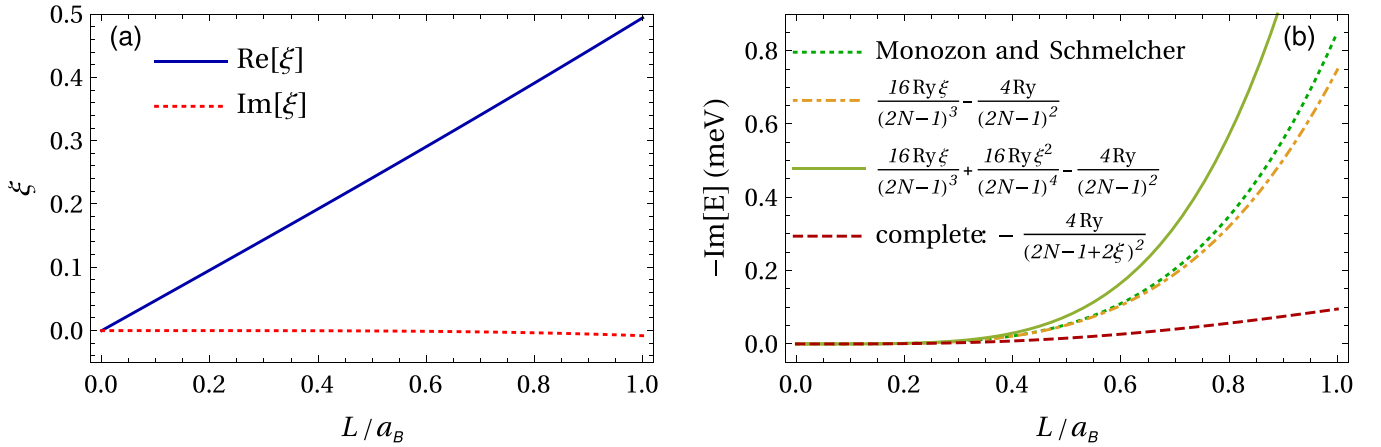


FIG. 7. (a) Values of ξ as a function of L/a_B . (b) The imaginary part of the complex energy, i.e., the linewidth, calculated using the complete expressions derived in Ref. [38], see Eqs. (14) and (A1), and different applied approximations, also including the original result by Monozon and Schmelcher.

subband was studied. We obtained that the resonant states corresponding to the second quantum-confinement subband have negligibly small linewidths. Thus, they can be regarded as examples of the bound states in the continuum. The linewidths of the states associated with the third quantum-confinement subband are nonzero. For $L \leq 1$ nm, the calculated values of the linewidth scale with L approximately as L^4 , which is in agreement with results obtained by Monozon and Schmelcher in Ref. [38]. For QW widths $L = 1.2\text{--}50$ nm, the linewidth broadens linearly with an increase of L , then it flattens out and saturates at about 0.5 meV for $L \sim 100$ nm. With the further growth of L , the linewidth diminishes and should completely vanish when the energy of the corresponding state transfers to the discrete part of the spectrum. We extended the results obtained in Ref. [38] for very narrow QWs, $L \ll a_B$ to the QW of the thickness of order of the impurity's Bohr radius a_B and larger by providing new numerical data on $\hbar\Gamma$ of resonant states of the third quantum-confinement subband. We also showed how one can apply the complete expressions derived in Ref. [38] without approximations to obtain more precise magnitudes of the linewidths of the resonant states for QW widths of order of the Bohr radius. Additionally, we calculated the linewidths for the case when the electron impurity is localized away from the center of the QW.

The numerical methods of this paper can be applied to the model of the excitons in cuprous oxide QWs [82]. The obtained results are also important for contemporary experimental studies of Cu_2O -based heterostructures [83]. The estimations and the dependencies of the linewidth broadenings on the QW width provide valu-

able information for spectroscopy measurements of these structures.

ACKNOWLEDGMENTS

The author is grateful to Professor Jörg Main and his research group for the stimulating discussions and careful reading of the manuscript. The author is indebted to Professor B. S. Monozon and Professor P. Schmelcher for the particular attention to the current work and for organization of the dedicated on-site seminar in Hamburg on November 15, 2021. Financial support from the Russian Science Foundation (Grant No. 19-72-20039) is acknowledged. Calculations were carried out using the facilities of the Resource Center “Computer Center of SPbU.”

APPENDIX

Here we outline the theoretical results of Ref. [38] and show in detail how they can be improved for $L \sim a_B$ if one calculates the linewidths using the complete expressions in Ref. [38] instead of taking the lowest-order approximations to obtain the analytical results.

In Ref. [38] the model of three quantum-confinement subbands in QW with infinite barriers was solved. Within this model, the complex energies of the electron impurity are defined by the parameter ξ via Eq. (14). For $L \ll a_B$, this parameter is assumed to be small enough to approximate the energies by the constant and the linear in ξ terms, see the right-hand side of Eq. (14). Monozon and Schmelcher found that ξ can, in turn, be given by the ratio of perturbation series in the small parameter L/a_B :

$$\xi = \frac{g_{33}}{2} \frac{1 + \frac{i\pi}{4}(g_{11} + g_{22}) - \frac{\pi^2}{16}g_{11}g_{22}}{1 + \frac{i\pi}{4}(g_{11} + g_{22}) - \frac{1}{4}(g_{31}^2 + g_{32}^2) - \frac{i\pi}{16}(g_{22}g_{31}^2 + g_{11}g_{32}^2) - \frac{\pi^2}{16}g_{11}g_{22}}. \quad (\text{A1})$$

Here the integrals are given as

$$g_{jk} = \left\langle \psi_j(z) \left| \frac{4|z-b|}{a_B} \right| \psi_k(z) \right\rangle.$$

For QW with infinite barriers, the integrals include the well-known wave functions (5) and are evaluated exactly:

$$\begin{aligned} g_{11} &= \left(\frac{L}{a_B}\right) \left[1 + \frac{4}{\pi^2} [(t/2)^2 - \cos^2(t/2)] \right], \\ g_{22} &= \left(\frac{L}{a_B}\right) \left[1 + \frac{1}{\pi^2} (t^2 - \sin^2 t) \right], \\ g_{33} &= \left(\frac{L}{a_B}\right) \left[1 + \frac{4}{9\pi^2} [(3t/2)^2 - \cos^2(3t/2)] \right], \\ g_{32} &= \left(\frac{L}{a_B}\right) \frac{1}{\pi^2} \left[\frac{8}{25} \sin(5t/2) - 8 \sin(t/2) \right], \\ g_{31} &= \left(\frac{L}{a_B}\right) \frac{4}{\pi^2} \cos^4(t/2), \end{aligned}$$

where $t = 2\pi b/L$. For $L \ll a_B$, the series in Eq. (A1) can be truncated leaving only the leading orders of L/a_B which are necessary to obtain the unknown quantity analytically. By doing likewise, as well as by using the linear approximation in Eq. (14), Monozon and Schmelcher obtained the following approximations for the real part of the complex energy (the energy shift):

$$\begin{aligned} \Delta E_{\text{Re}} &= \frac{8\text{Ry}}{(2N-1)^3} g_{33} \left[1 + \frac{1}{4} (g_{31}^2 + g_{32}^2) \right] = \frac{8\text{Ry}}{(2N-1)^3} \left(\frac{L}{a_B}\right) \left[1 + \frac{4}{9\pi^2} [(3t/2)^2 - \cos^2(3t/2)] \right] \\ &\times \left\{ 1 + \frac{1}{4} \left(\frac{L}{a_B}\right)^2 \left[\frac{16}{\pi^4} \cos^8(t/2) + \frac{1}{\pi^4} \left(\frac{8}{25} \sin(5t/2) - 8 \sin(t/2) \right)^2 \right] \right\} \end{aligned} \quad (\text{A2})$$

and for the imaginary part (the linewidth)¹

$$\begin{aligned} \Delta E_{\text{Im}} &= -\frac{i\pi\text{Ry}}{2(2N-1)^3} g_{33} [g_{11}g_{31}^2 + g_{22}g_{32}^2] = -\frac{i}{\pi^3} \frac{8\text{Ry}}{(2N-1)^3} \left(\frac{L}{a_B}\right)^4 \left[1 + \frac{4}{9\pi^2} [(3t/2)^2 - \cos^2(3t/2)] \right] \\ &\times \left\{ \left[1 + \frac{4}{\pi^2} [(t/2)^2 - \cos^2(t/2)] \right] \cos^8(t/2) + \left[1 + \frac{1}{\pi^2} (t^2 - \sin^2 t) \right] \left[\frac{2}{25} \sin(5t/2) - 2 \sin(t/2) \right]^2 \right\}. \end{aligned} \quad (\text{A3})$$

These are Eqs. (11) and (12) for arbitrary b . The generalizations of Eqs. (8) and (9) can be found in Ref. [38].

Using all the terms in Eq. (A1) we can evaluate ξ for different ratios L/a_B . The dependence $\xi(L/a_B)$ is shown in Fig. 7(a). One can see that already for $L/a_B = 0.3$, the quantity 2ξ in the denominator of $E_{e3,Ns} = -4\text{Ry}/(2N-1+2\xi)^2$ is of about 0.3, which is not so small comparing to unity. Simultaneously, the last, quadratic in ξ , term in Eq. (14) starts playing a role for such L , because, due to the large real part, its imaginary part becomes of the order of $\text{Im}[\xi]$. Thus, the linear in ξ approximation becomes reasonably inappropriate.

We evaluate the complex energies for $L < a_B$ by different ways to compare. To do it, we calculate ξ using all the terms in Eq. (A1) and use it further to calculate the complex energy by the complete equation $E_{e3,Ns} = -4\text{Ry}/(2N-1+2\xi)^2$ as well as by the linear and quadratic approximations on the

right-hand side of Eq. (14). The comparison of the imaginary parts, the linewidths, of the obtained values with the result by Monozon and Schmelcher is shown in Fig. 7(b). For small values of L/a_B both shown curves coincide, however for $L \sim a_B$ there is a significant difference. Using all the available terms in Eq. (A1) to evaluate ξ and calculating exactly the energy as $E_{e3,Ns} = -4\text{Ry}/(2N-1+2\xi)^2$ allows us to significantly improve the approximation of the imaginary part of the complex energy for $L \sim a_B$. We see in Fig. 5 that for $L \sim a_B$ the results obtained from the total expression for ξ and the complete equation for $E_{e3,Ns}$ give linewidths which agree better with our numerical data. There is also the linear-like dependence of this quantity for such values of L .

As a result, we see that the complete expressions for ξ and $E_{e3,Ns}$ significantly improve theoretical predictions for the linewidths for $L \sim a_B$.

¹Please note the two times difference with Γ in Ref. [38] due to the definition of the complex energy as $E - i\Gamma/2$ there.

[1] J. M. Luttinger, *Phys. Rev.* **102**, 1030 (1956).

[2] F. Bassani, G. Iadonisi, and B. Preziosi, *Phys. Rev.* **186**, 735 (1969).

[3] A. Baldereschi and N. O. Lipari, *Phys. Rev. B* **3**, 439 (1971).

[4] E. L. Ivchenko, *Optical Spectroscopy of Semiconductor Nanostructures* (Alpha Science, Harrow, 2005).

[5] E. O. Göbel, H. Jung, J. Kuhl, and K. Ploog, *Phys. Rev. Lett.* **51**, 1588 (1983).

- [6] M. Tsuchiya, T. Matsusue, and H. Sakaki, *Phys. Rev. Lett.* **59**, 2356 (1987).
- [7] B. Deveaud, F. Clérot, A. Regreny, and K. Fujiwara, *Superlattices Microstruct.* **8**, 85 (1990).
- [8] P. J. Bishop, M. E. Daniels, B. K. Ridley, and K. Woodbridge, *Phys. Rev. B* **45**, 6686 (1992).
- [9] R. F. Kazarinov and R. A. Suris, *Fiz. Tekh. Poluprovodn.* **5**, 797 (1971).
- [10] J. Faist, F. Capasso, D. L. Sivco, C. Sirtori, A. L. Hutchinson, and A. Y. Cho, *Science* **264**, 553 (1994).
- [11] W. W. Chow and S. W. Koch, *Semiconductor-Laser Fundamentals* (Springer, Berlin, 1999).
- [12] Zh. I. Alferov, *Semiconductors* **32**, 1 (1998).
- [13] R. Köhler, A. Tredicucci, F. Beltram, H. E. Beere, E. H. Linfield, A. G. Davies, D. A. Ritchie, R. C. Iotti, and F. Rossi, *Nature (London)* **417**, 156 (2002).
- [14] D. A. Firsov, V. A. Shalygin, V. Yu. Panevin, G. A. Melentyev, A. N. Sofronov, L. E. Vorobjev, A. V. Andrianov, A. O. Zakhar'in, V. S. Mikhrin, A. P. Vasil'ev, A. E. Zhukov, L. V. Gavrilenko, V. I. Gavrilenko, A. V. Antonov, and V. Ya. Aleshkin, *Semiconductors* **44**, 1394 (2010).
- [15] M. Wienold, B. Röben, L. Schrottke, R. Sharma, A. Tharaoui, K. Biermann, and H. T. Grahn, *Opt. Express* **22**, 3334 (2014).
- [16] K. Fujita, S. Jung, Y. Jiang, J. H. Kim, A. Nakanishi, A. Ito, M. Hitaka, T. Edamura, and M. A. Belkin, *Nanophotonics* **7**, 1 (2018).
- [17] I. S. Makhov, V. Yu. Panevin, D. A. Firsov, L. E. Vorobjev, A. P. Vasil'ev, and N. A. Maleev, *J. Lumin.* **210**, 352 (2019).
- [18] G. Bastard, *Phys. Rev. B* **24**, 4714 (1981).
- [19] G. Bastard, *Phys. Rev. B* **30**, 3547 (1984).
- [20] G. Bastard, E. E. Mendez, L. L. Chang, and L. Esaki, *Phys. Rev. B* **26**, 1974 (1982).
- [21] D. B. Tran Thoai, R. Zimmermann, M. Grundmann, and D. Bimberg, *Phys. Rev. B* **42**, 5906(R) (1990).
- [22] A. V. Kavokin, J. J. Baumberg, G. Malpuech, and F. P. Laussy, *Microcavities* (Oxford University Press, Oxford, 2007).
- [23] V. A. Shuvayev, L. I. Deych, I. V. Ponomarev, and A. A. Lisyansky, *Superlattices Microstruct.* **40**, 77 (2006).
- [24] H. Haug and S. W. Koch, *Quantum Theory of the Optical and Electronic Properties of Semiconductors* (World Scientific, Singapore, 2009).
- [25] J. L. Birman, R. G. Nazmitdinov, and V. I. Yukalov, *Phys. Rep.* **526**, 1 (2013).
- [26] T. C. H. Liew, M. M. Glazov, K. V. Kavokin, I. A. Shelykh, M. A. Kaliteevski, and A. V. Kavokin, *Phys. Rev. Lett.* **110**, 047402 (2013).
- [27] E. S. Khrantsov, P. A. Belov, P. S. Grigoryev, I. V. Ignatiev, S. Yu. Verbin, Yu. P. Efimov, S. A. Eliseev, V. A. Lovtcius, V. V. Petrov, and S. L. Yakovlev, *J. Appl. Phys.* **119**, 184301 (2016).
- [28] D. K. Loginov, P. A. Belov, V. G. Davydov, I. Ya. Gerlovin, I. V. Ignatiev, A. V. Kavokin, and Y. Masumoto, *Phys. Rev. Research* **2**, 033510 (2020).
- [29] R. L. Greene, K. K. Bajaj, and D. E. Phelps, *Phys. Rev. B* **29**, 1807 (1984).
- [30] B. Li, A. F. Schlachmuylders, B. Partoens, W. Magnus, and F. M. Peeters, *Phys. Rev. B* **77**, 115335 (2008).
- [31] D. G. W. Parfitt and M. E. Portnoi, *J. Math. Phys.* **43**, 4681 (2002).
- [32] P. Duclos, P. Stovicek, and M. Tusek, *J. Phys. A: Math. Theor.* **43**, 474020 (2010).
- [33] P. A. Belov, *Phys. E* **112**, 96 (2019).
- [34] C. Priester, G. Allan, and M. Lannoo, *Phys. Rev. B* **29**, 3408 (1984).
- [35] S. T. Yen, *Phys. Rev. B* **66**, 075340 (2002).
- [36] A. Blom, M. A. Odnoblyudov, I. N. Yassievich, and K. A. Chao, *Phys. Rev. B* **68**, 165338 (2003).
- [37] V. Ya. Aleshkin and L. V. Gavrilenko, *J. Exp. Theor. Phys.* **98**, 1174 (2004).
- [38] B. S. Monozon and P. Schmelcher, *Phys. Rev. B* **71**, 085302 (2005).
- [39] V. Ya. Aleshkin, L. V. Gavrilenko, M. A. Odnoblyudov, and I. N. Yassievich, *Semiconductors* **42**, 880 (2008).
- [40] U. Fano, *Phys. Rev.* **124**, 1866 (1961).
- [41] A. E. Miroshnichenko, S. Flach, and Y. S. Kivshar, *Rev. Mod. Phys.* **82**, 2257 (2010).
- [42] G. F. Gliniskii, V. A. Lakisov, A. G. Dolmatov, and K. O. Kravchenko, *Nanotechnology* **11**, 233 (2000).
- [43] P. A. Belov and E. S. Khrantsov, *J. Phys.: Conf. Ser.* **816**, 012018 (2017).
- [44] B. S. Monozon, private communication, Hamburg, November 15, 2021.
- [45] H. Feshbach, *Ann. Phys.* **5**, 357 (1958).
- [46] H. Friedrich and D. Wintgen, *Phys. Rev. A* **31**, 3964 (1985).
- [47] P. S. Grigoryev, A. S. Kurdyubov, M. S. Kuznetsova, I. V. Ignatiev, Yu. P. Efimov, S. A. Eliseev, V. V. Petrov, V. A. Lovtcius, and P. Yu. Shapochkin, *Superlattices Microstruct.* **97**, 452 (2016).
- [48] A. V. Trifonov, S. N. Korotan, A. S. Kurdyubov, I. Ya. Gerlovin, I. V. Ignatiev, Yu. P. Efimov, S. A. Eliseev, V. V. Petrov, Yu. K. Dolgikh, V. V. Ovsyankin, and A. V. Kavokin, *Phys. Rev. B* **91**, 115307 (2015).
- [49] E. Kamenetskii, A. Sadreev, and A. Miroshnichenko, *Fano Resonances in Optics and Microwaves: Physics and Applications* (Springer, Berlin, 2018).
- [50] C. W. Hsu, B. Zhen, A. D. Stone, J. D. Joannopoulos, and M. Soljacic, *Nat. Rev. Mater.* **1**, 16048 (2016).
- [51] N. Rivera, C. W. Hsu, B. Zhen, H. Buljan, J. D. Joannopoulos, and M. Soljacic, *Sci. Rep.* **6**, 33394 (2016).
- [52] F. H. Stillinger and D. R. Herrick, *Phys. Rev. A* **11**, 446 (1975).
- [53] R. Y. Kezerashvili, *Few-Body Syst.* **60**, 52 (2019).
- [54] P. A. Belov and S. L. Yakovlev, *Springer Proc. Phys.* **238**, 29 (2020).
- [55] N. Moiseyev, *Phys. Rep.* **302**, 212 (1998).
- [56] J. Aguilar and J. M. Combes, *Commun. Math. Phys.* **22**, 269 (1971).
- [57] E. Balslev and J. M. Combes, *Commun. Math. Phys.* **22**, 280 (1971).
- [58] B. Simon, *Commun. Math. Phys.* **27**, 1 (1972).
- [59] B. Simon, *Phys. Lett. A* **71**, 211 (1979).
- [60] N. Moiseyev, P. R. Certain, and F. Weinhold, *Mol. Phys.* **36**, 1613 (1978).
- [61] Y. K. Ho, *Phys. Rep.* **99**, 1 (1983).
- [62] V. I. Kukulin, V. M. Krasnopolsky, and J. Horáček, *Theory of Resonances: Principles and Applications* (Springer, Berlin, 1989).
- [63] N. Elander and E. Yarevsky, *Phys. Rev. A* **57**, 3119 (1998).
- [64] D. A. Telnov, K. E. Sosnova, E. Rozenbaum, and S.-I. Chu, *Phys. Rev. A* **87**, 053406 (2013).

- [65] V. V. Serov, V. L. Derbov, T. A. Sergeeva, and S. I. Vinitzky, *Phys. Rev. A* **88**, 043403 (2013).
- [66] T. Myo, Y. Kikuchi, H. Masui, and K. Kato, *Prog. Part. Nucl. Phys.* **79**, 1 (2014).
- [67] P. A. Belov, *Semiconductors* **53**, 2049 (2019).
- [68] H. C. Kamban and T. G. Pedersen, *Phys. Rev. B* **100**, 045307 (2019).
- [69] P. Zielinski, P. Rommel, F. Schweiner, and J. Main, *J. Phys. B: At. Mol. Opt. Phys.* **53**, 054004 (2020).
- [70] P. Rommel, P. Zielinski, and J. Main, *Phys. Rev. B* **101**, 075208 (2020).
- [71] P. Rommel, J. Main, S. O. Krüger, and S. Scheel, *Phys. Rev. B* **104**, 085204 (2021).
- [72] I. Vurgaftman, J. R. Meyer, and L. R. Ram-Mohan, *J. Appl. Phys.* **89**, 5815 (2001).
- [73] L. D. Landau and E. M. Lifshits, *Quantum Mechanics. Nonrelativistic Theory* (Nauka, Moscow, 2004).
- [74] K. Rapedius, *Eur. J. Phys.* **32**, 1199 (2011).
- [75] M. V. Volkov, N. Elander, E. Yarevsky, and S. L. Yakovlev, *Europhys. Lett.* **85**, 30001 (2009).
- [76] P. A. Belov, V. A. Gradusov, M. V. Volkov, S. L. Yakovlev, and E. A. Yarevsky, *Few-Body Syst.* **58**, 114 (2017).
- [77] T. N. Rescigno, M. Baertschy, D. Byrum, and C. W. McCurdy, *Phys. Rev. A* **55**, 4253 (1997).
- [78] V. G. Korneev and U. Langer, *Dirichlet-Dirichlet Domain Decomposition Methods for Elliptic Problems* (World Scientific, Singapore, 2015).
- [79] P. A. Belov, E. R. Nugumanov, and S. L. Yakovlev, *J. Phys.: Conf. Ser.* **929**, 012035 (2017).
- [80] D. C. Sorensen, R. B. Lehoucq, and P. Vu, *ARPACK: An Implementation of the Implicitly Restarted Arnoldi Iteration That Computes Some of the Eigenvalues and Eigenvectors of a Large Sparse Matrix* (Rice University, Houston, 1995).
- [81] P. J. Pearah, J. Klem, T. Henderson, C. K. Peng, H. Morkoc, D. C. Reynolds, and C. W. Litton, *J. Appl. Phys.* **59**, 3847 (1986).
- [82] D. Ziemkiewicz, G. Czajkowski, K. Karpinski, and S. Zielinska-Raczynska, *Phys. Rev. B* **104**, 075303 (2021).
- [83] A. Konzelmann, B. Frank, and H. Giessen, *J. Phys. B: At. Mol. Opt. Phys.* **53**, 024001 (2020).